



Theoretical and experimental study of FeSi on magnetic and phase properties

J. F. Piamba^{1,2} · C. Ortega^{3,4} · R. Hernández-Bravo⁴ · J. M. González Carmona^{3,4} · J. A. Tabares¹ · G. A. Pérez Alcázar¹ · J. M. Alvarado-Orozco⁴

Received: 9 April 2020 / Accepted: 29 September 2020 / Published online: 10 October 2020
© Springer-Verlag GmbH Germany, part of Springer Nature 2020

Abstract

In the present work, the structural, magnetic, and theoretical analysis of the Fe–Si alloy prepared by melting and heat-treated was performed. The ordered FeSi simple cubic (sc) phase was obtained by melting and heat treatment processes as determined by X-ray diffraction. The presence of the superstructure peak in the (312) crystalline direction confirms the high structural order reached. Using Mössbauer spectrometry (MS), a paramagnetic behavior with quadrupole splitting of $SQ = 0.53 \pm 0.02$ mm/s was obtained. Although MS indicates paramagnetic behavior, vibrating sample magnetometry (VSM) showed ferromagnetic behavior with a coercive field of 25 Oe, associated with a small amount of Fe₃Si segregations detected by scanning electron microscopy/energy dispersive spectrometry (SEM/EDS). Using density functional theory (DFT), the crystalline structures for the simple cubic (sc) Fe₅₀Si₅₀, face-centered cubic (fcc) Fe₃Si, and body-centered cubic (bcc) Fe₃Si crystalline structures were simulated. Electron total density values were calculated to perform energetic comparisons with magnetic behavior. The electronic structures and magnetic properties of the Fe–Si alloys in different stoichiometric configurations were calculated by CASTEP, which employed first principles DFT. The density of states (DOS) and band structures were calculated together with magnetic properties. The results showed that the high value of the polarization spin for the fcc and bcc structures is due to the contribution of the high amount of Fe atoms above the Si atoms, which is reflected in an increase in the magnetic moment and that their presence could explain the ferromagnetic behavior observed by VSM.

Keywords Mössbauer spectrometry · X-ray diffraction · Spin-polarized density functional theory (DFT) calculations · Scanning electron microscopy (SEM)

1 Introduction

During the last years, the study of the magnetic and electronic transport properties of new materials has been of great interest inside the scientific community, looking for their possible applications. The research on this type of materials has focused on the ability to synthesize them in such a way to obtain a significant effect of spin polarization [1]. The recent advances performed in the field of electronics have served to study the influence of spin over the conducting properties. It is a field that is currently booming, and its development would be very successful if fully rotationally polarized materials could be developed.

Studies related to spin polarization in the framework of the density functional theory (DFT) have become a powerful tool to describe the magnetic properties of solid-state materials [2]. These calculations allow us to obtain a quantitative base of the spin behavior and predict the different

✉ J. F. Piamba
jeferson.piamba@correounivalle.edu.co

J. A. Tabares
jesus.tabares@correounivalle.edu.co

¹ Departamento de Física, Universidad del Valle, A.A. 25360, Cali, Colombia

² Facultad de Ciencias Naturales y Matemáticas, Universidad de Ibagué, Tolima, 730002 Ibagué, Colombia

³ Grupo de Investigación “Recubrimientos Duros y Aplicaciones Industriales RDAI”, Facultad de Ingeniería, Universidad del Valle, A.A. 25360, Cali, Colombia

⁴ CONACYT-Centro de Ingeniería y Desarrollo Industrial CIDESI, Av. Playa, Av Pie de la Cuesta No. 702, Desarrollo San Pablo, 76125 Santiago de Querétaro, Qro, Mexico

mechanisms that lead to the magnetism appearance. Magnetism in transition metals occurs mainly due to the competition between the electronic spin-exchange interaction energy of the 3d electrons and the thermal one. In order that magnetism occurs, the electrons must be located within the electronic 3d states, as observed in well-known metals like iron (Fe), cobalt (Co), and nickel (Ni).

Binary alloys have been widely studied for various applications, mainly Fe–Si alloys [3–6], in their cubic structure due to their paramagnetic behavior. The high permeability of Fe–Si alloys and low Si concentrations are essential characteristics of this type of alloys that make it very efficient for the development of better electronic devices, transformers, and flow multipliers. During a previous work on Fe₅₀Si₅₀ alloys [6], the formation of different Fe–Si phases was observed, for example, sc, and bcc, when the alloy was prepared by mechanical alloying for 48 h [7]. This sample was synthesized for 72 h at 750 °C, obtaining the paramagnetic FeSi (sc) and Fe₅Si₃ phases, where the latter is the most stable at high temperatures and is called the η phase. When the sample was ground at different moments of the experiment, it was possible to observe the absence of a high-temperature bcc Fe–Si phase (α phase), in turn joining with the FeSi phase (sc). If the milling time is increased considerably, both phases become disordered. However, the Fe_x–Si_y system has several phases [8], which can crystallize depending on the used temperature during the synthesis: β -FeSi₂ semiconductor, which is amorphous [9], nanocrystalline (NC)–FeSi₂ [10], and FeSi metallic nonmagnetic [11].

On the other hand, it has been highlighted by Al-Sharif et al. [12] that there are several reasons to consider the equiatomic FeSi compound as an interesting material, among them the rapidly increasing of magnetic susceptibility at low temperatures with a full maximum at 500 K, which can be considered as a particular magnetic property. In this respect, the application of computational simulations is of great interest for obtaining electronic properties that explain the unusual magnetic behavior of this material. The recent advances have been found based on the first principles density functional study on the Fe–Mo double Perovskites, as was reported by Carvajal et al. [13]. The results showed that valence and conduction bands are formed by bonding and antibonding crystalline orbitals arising from combinations of Fe and Mo d orbital with O p ones. Masrour et al. [14] studied electronic and magnetic properties, and phase diagrams of systems with the Fe₄N structure by ab initio calculations and Monte Carlo method. The results showed that a clear two-step hysteresis loop could be observed, typical for the mixed 1 and 3/2 spin Ising model with Fe₄N structure. Gu et al. [15] used density functional calculations on the Fe–Pt system's electronic and magnetic properties from the band structure and density of states analysis. The results showed that when Pt concentration increases, Fe 4s, and 3d electrons

decrease while 4p electrons increase, and the magnetic moment of Fe atom increases. Pt atoms also contribute to the magnetic moment due to polarization. Cardoso Schwindt et al. [16] studied the electronic structure, chemical bonding, and magnetism on FeSiAl alloy using density functional theory (DFT). These calculations were performed to understand the magnetic properties of this alloy. The results showed that magnetic moments of Fe atoms decrease due to the effect of Si and Al. The DOS and band structure reveals the stabilization of Fe, Si, and Al bands. Nazir et al. [17] studied the structural, electronic, and magnetic properties of ZnS and CdS alloyed with 25% Cr, and could show the stability of the ferromagnetic spin state versus the antiferromagnetic state.

Based on all these investigations, our work aims to study the Fe–Si different phase behaviors and how they affect its stability and electronic and magnetic properties. From Mössbauer spectrometry (MS), X-ray diffraction (XRD), vibrating sample magnetometry (VSM), and density functional theory (DFT) calculations we study the magnetic behavior of FeSi in the sc, fcc, and bcc phases. In this work, we present a detailed study of the electronic structure and magnetization of FeSi (sc and fcc) within generalized gradient approximation (GGA) using self-consistent full-potential methods. Many experimental works are found in the literature for compositions near the Fe₅₀Si₅₀, but the theoretical calculations of current work, applying the first principle density functional theory (DFT) method, reported, by the first time, the electronic properties of the phases around the equiatomic composition, explaining in this way their magnetic behavior.

2 Experimental methodology

2.1 Sample preparation and characterization techniques

The samples were prepared by using high purity Fe and Si powders (> 99.9%). Samples of 3.0 g were prepared by arc melting in an argon atmosphere, followed by heat treatment. The heat treatment process was carried out by first, encapsulating the obtained pellet, after the melting process, in an evacuated quartz tube under an argon atmosphere, and then increasing the temperature up to 900 °C to homogenize the sample and to establish the sc structure, and then keeping it at 750 °C for 72 h to permit its ordering. Mössbauer Spectroscopy measurements were conducted in a conventional spectrometer with a ⁵⁷Co(Rh) source of 25 mCi. The Mössbauer spectra were fitted using the MOSFIT program [18], and the hyperfine parameters were referred to pure α -Fe. The XRD patterns were registered in a Bruker D8 ADVANCE diffractometer using a CuK α source and a graphite monochromator in the detector entry. The calibration sample was Si. The patterns were taken from 20.00 up to 85.00°, in steps

of 0.02° every 5 s. The patterns were refined by using the GSAS program [19] applying the Rietveld method. The VSM measure was realized between ± 2.0 T with a magnetic field variation rate of 50 Oe/s at 300 K in a PPMS of quantum design system.

2.2 Theoretical methodology

The electronic properties of FeSi were studied within the density functional theory (DFT) framework. Generalized gradient approximation (GGA) with Perdew–Burke–Ernzerhof (PBE) was used within the Cambridge sequential total energy package (CASTEP) code [20, 21]. The electron and core interactions are included using the ultrasoft pseudopotential. Among the ultrasoft pseudopotentials available in CASTEP are included the necessary parameters for the inclusion of the spin–orbit coupling essential for relativistic correction [22]. Depending on the computational tool available, the Coulomb U energy and the J exchange energy, known as the Hubbard potential, are combined into a single parameter known as the Coulomb U repulsion on site, which are included in the computational code within the CASTEP platform. DFT+ U calculations were performed for spin polarization [23, 24]. Atomic positions were optimized until the residual forces were 0.01 eV/Å. The integration in the Brillouin zone has been done on special k points ($8 \times 8 \times 8$ Monkhorst–Pack grid) determined according to the Monkhorst–Pack scheme with a cutoff energy of 330 eV.

To investigate the Fe–Si alloy, the simple cubic (sc) FeSi, the face-centered cubic (fcc) Fe_3Si , and the body-centered cubic (bcc) Fe_3Si structures were used. Figure 1 illustrates the cubic cell structure of FeSi constructed from the XRD results and molecular modeling. The lattice parameters,

density of states (DOS), and electronic band structure or simply band structure were obtained in our calculations.

The DOS plays a vital role in the analysis of the physical properties of materials. In solid state and condensed matter physics, the DOS of a system describes the number of states per interval of energy at each energy level that is available to be occupied. A high DOS at a specific energy level means that there are many available states for occupation. A DOS of zero means that no states can be occupied at that energy level. Band structures describe the range of energies of an electron that is within the solid material.

3 Results and discussion

The melting and heat treatment processes allowed us to obtain and consolidate the ordered FeSi simple cubic (sc) phase, which is of the B20 structure. By X-ray diffraction, we found that the system presents a FeSi mono-phasic sc structure (see Fig. 2), with parallel and perpendicular crystallite size of 574.2 ± 0.5 (nm) and 209.6 ± 0.5 (nm), respectively, and a lattice parameter of 4.489 ± 0.003 (Å).

The FeSi system's metallography shows uniformity and homogeneity of material related to tonality and texture (see Fig. 3a). Figure 3b shows some lighter small areas and large dark areas, to identify the difference in composition between them, SEM–EDS measurements were performed.

In agreement with the results obtained by X-ray diffraction, the large dark areas must correspond to the FeSi sc phase, while the small light areas are related to phases rich in Fe, an element with a higher atomic number than Si. It is possible that the phase percentage of the clear zone is less than the detection limit of X-ray diffraction. The results of SEM–EDS of Fig. 4 indicate that the average

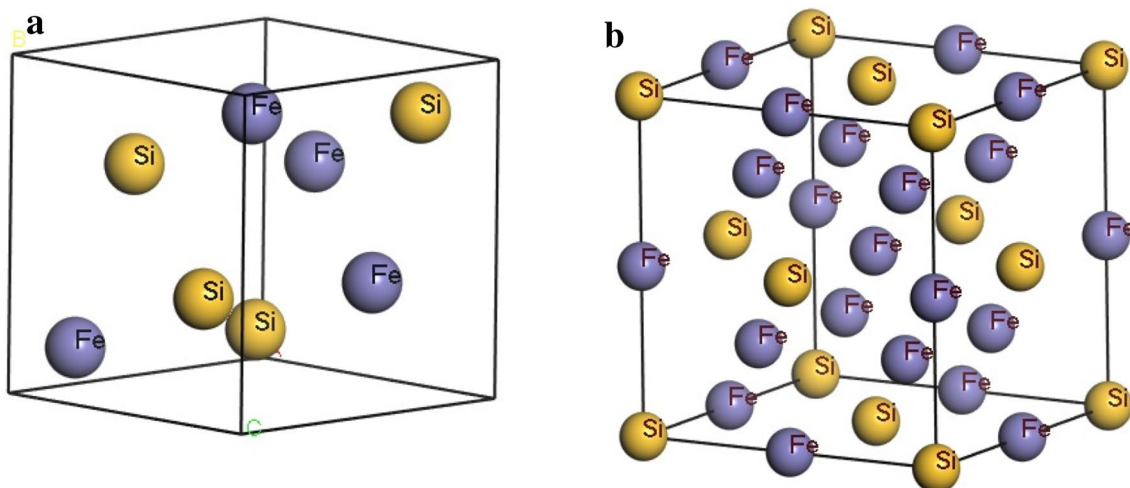


Fig. 1 Cell structure for FeSi. **a** Simple cubic (primitive) structure. **b** Cubic sodium chloride structure (fcc)

Fig. 2 XRD pattern of the $\text{Fe}_{50}\text{Si}_{50}$ ordered sample

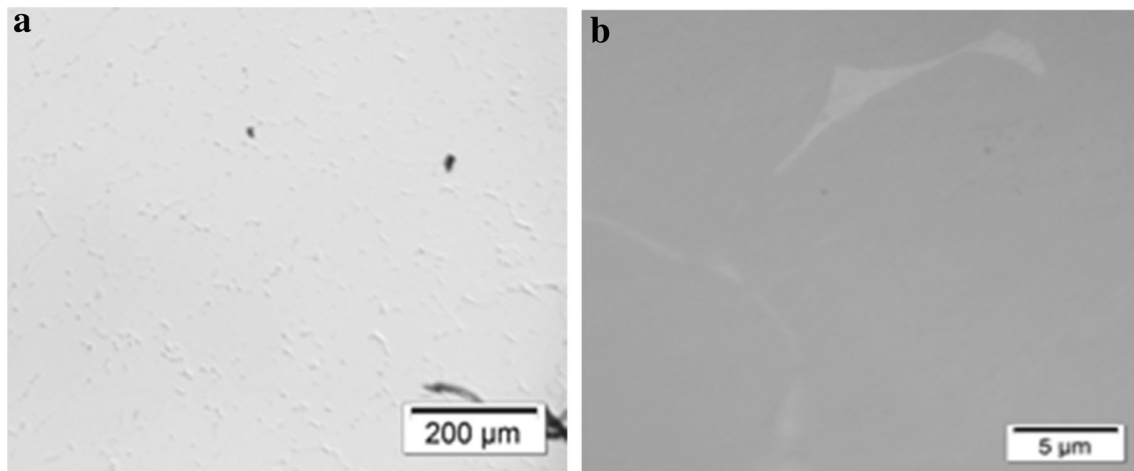
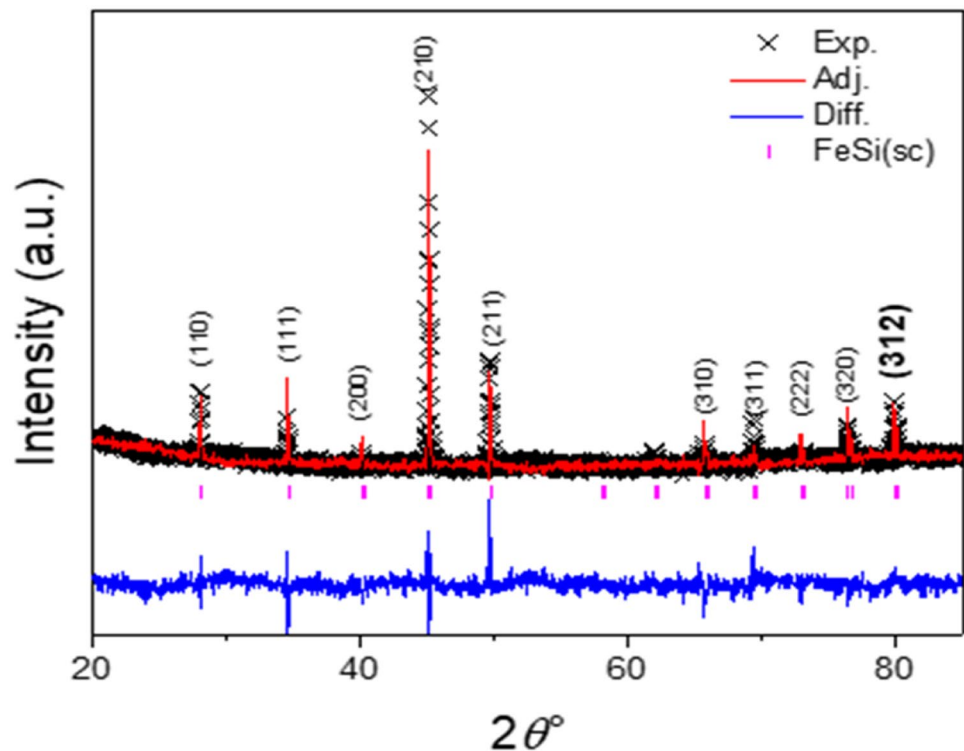


Fig. 3 Metallographic micrographs of $\text{Fe}_{50}\text{Si}_{50}$ prepared by melting and heat treatment. **a** General view, **b** image taken at $\times 200$ with evidence of the coexistence of two possible phases (dark: $\text{FeSi}(\text{sc})$, bright: Fe_3Si)

composition of light and dark areas is $\text{Fe}_{75.2}\text{Si}_{24.8}$ and $\text{Fe}_{51.8}\text{Si}_{48.2}$, respectively.

Figure 5 shows the Mössbauer spectrum obtained for the sample, that allows concluding that the $\text{FeSi}(\text{sc})$ system presents a paramagnetic behavior at room temperature, due its fitting includes one doublet with an isomer shift of $0.29(3)$ mm/s and a quadrupole splitting of $0.53(0)$ mm/s. This paramagnetic behavior has been reported in the same

system when it was produced by mechanical alloying at different milling times [25].

The VSM measurement shows that the hysteresis loop is narrow (see Fig. 6a), and after performing a zoom near the coordinates origin (Fig. 6b), it is observed that the coercive field (H_c) is 25.9 ± 0.2 Oe, which indicates the soft magnetic character of the sample.

Fig. 4 SEM image of FeSi sample

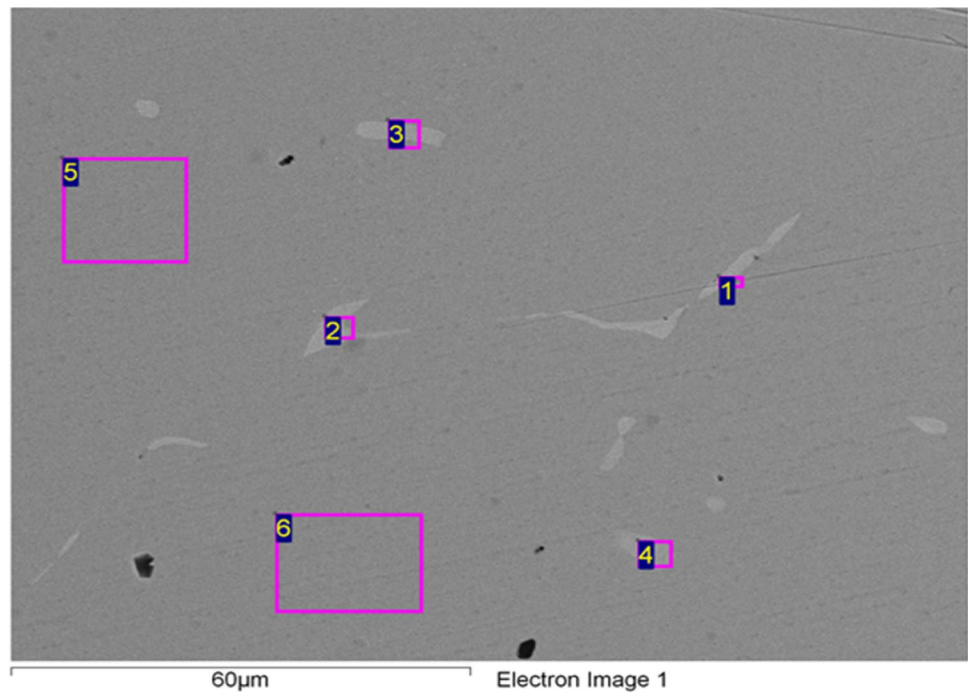
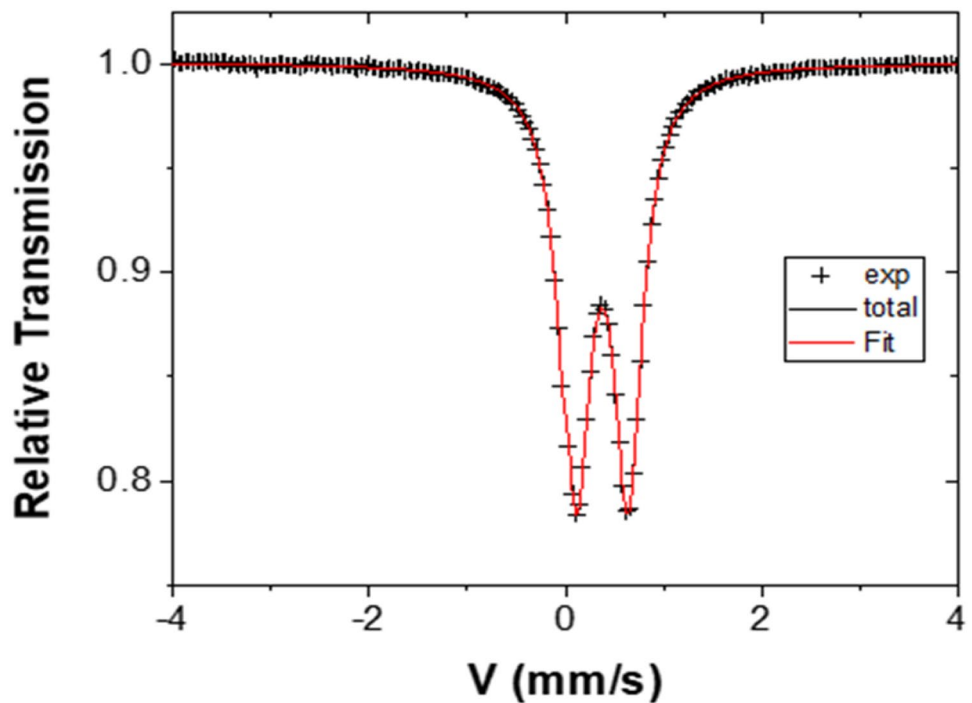


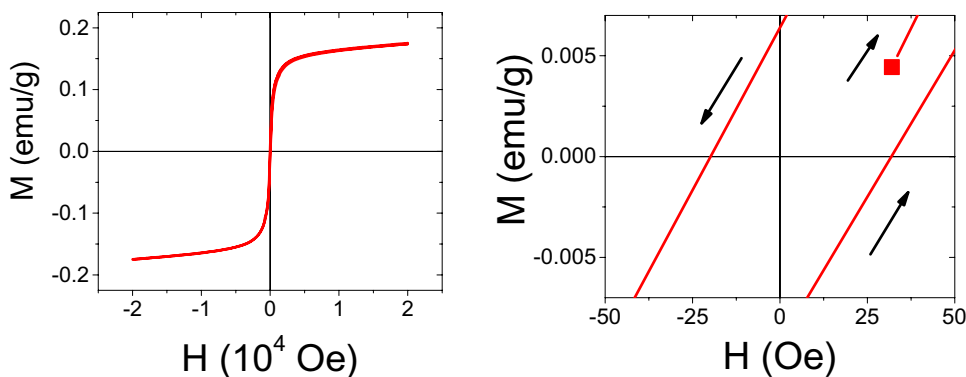
Fig. 5 Mössbauer spectrum of the FeSi (sc) system at RT



The fact that VSM measurement detected a weak ferromagnetism and Mössbauer measurement a paramagnetic behavior, could be attributed to the grain boundaries, in which the fact that VSM measurement detected a weak ferromagnetism and Mössbauer measurement a paramagnetic behavior could be attributed to the grain boundaries, in which the coherence is lost, and the coordination number

of Fe atoms is different to that inside the grains (crystallites). Probably, on the grain boundaries, it can appear less Fe–Si bonds than those inside the grains. Therefore, more Fe–Fe bonds are present on the grain boundaries, and, as it was shown in a recent study about $\text{Fe}_{50}\text{Si}_{50}$ samples milled at different times the grain boundaries are the places in which Fe_3Si crystallites begin to be formed. As it

Fig. 6 Hysteresis loop of FeSi sc system, **a** complete hysteresis loop, **b** zoom of the hysteresis loop around the origin



was reported in the literature, this phase is ferromagnetic [26–28].

From the hysteresis loops, the Thamm and Hesse plot was obtained [29]. For this, the hysteresis loop was normalized using the magnetization value at 2 T. The data from initial magnetization, demagnetization, and final magnetization curves 1, 2, and 3 respectively, were used and the average of loops 2 and 3 was found (Fig. 7a). Finally, the difference between curve 1 and the average was carried out, and this difference can be observed in Fig. 7b.

The result of Fig. 7b allows us to conclude that for small applied fields, the magnetization of the sample is contrary to the applied field, indicating that the main magnetic interaction between the magnetic moments of the particles is from the dipolar origin. This effect was also reported in films of magnetic recorders [27]. As for the case of a high applied field, the competition between the ferromagnetic exchange interaction and the dipole interaction is similar, and the δM values are near zero. It is possible that the magnetic moments of the small particles can be rotated to the applied field direction, contributing in this way to the exchange interaction of the atoms, and a competition of the dipolar interactions with the moments of the big particles could occur.

The XRD and Mössbauer results indicate the presence of one phase, with a simple cubic crystalline structure (with a paramagnetic behavior), while as, VSM and SEM/EDS suggest the presence of an additional phase with weak ferromagnetism associated to a bcc-D03 (Fe_3Si) type structure [26]. To complement these results, the band structure and the density of states of both structures were theoretically studied, i.e., sc- $\text{Fe}_{50}\text{Si}_{50}$ (paramagnetic), fcc- Fe_3Si (ferromagnetic), and bcc- Fe_3Si (ferromagnetic).

In Figs. 8, 9, and 10, the calculated density of states (DOS) and band structures for FeSi (sc), Fe_3Si (fcc), and Fe_3Si (bcc) are observed and Table 1 shows the energetic and thermodynamic values obtained from the simulation. These plots were obtained by the first-principle density functional theory with the polarization method. As only Fe has magnetic properties is; therefore, considered as spin-polarized, and for Si, the spin density is not restricted [30]. The obtained results indicate that the 3d electrons of the fcc and sc phases are close to the Fermi energy (represented as energy = 0). However, the peaks for the fcc and bcc structures (Figs. 9a, 10a) are larger than the sc one (Fig. 8a).

This may be because, in the fcc structure, the electrons with both up and down spin tend to be located near the Fermi level, and for the sc, the spins are delocalized: This

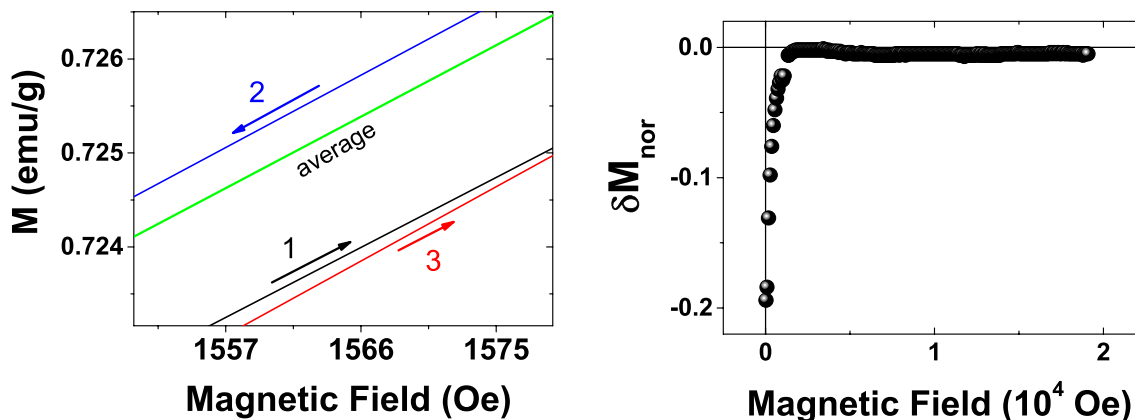


Fig. 7 **a** Zoom of hysteresis loop around to 1566 Oe of FeSi sample, **b** Thamm and Hesse plot

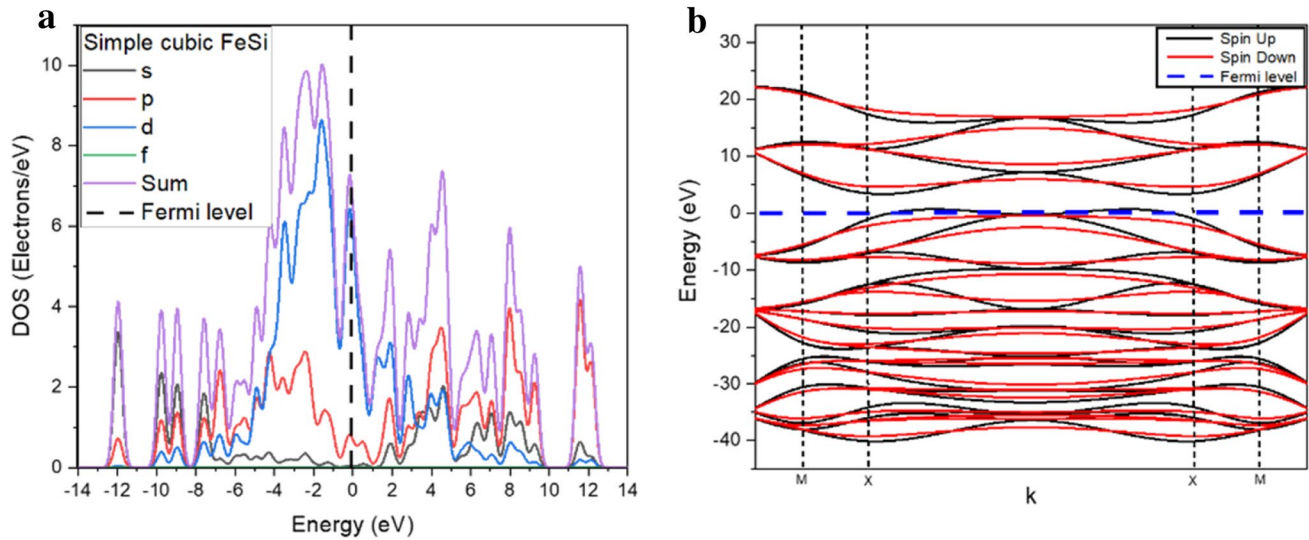


Fig. 8 **a** Total density of states (DOS) and **b** band structure of FeSi (sc) around the Fermi level (dotted line)

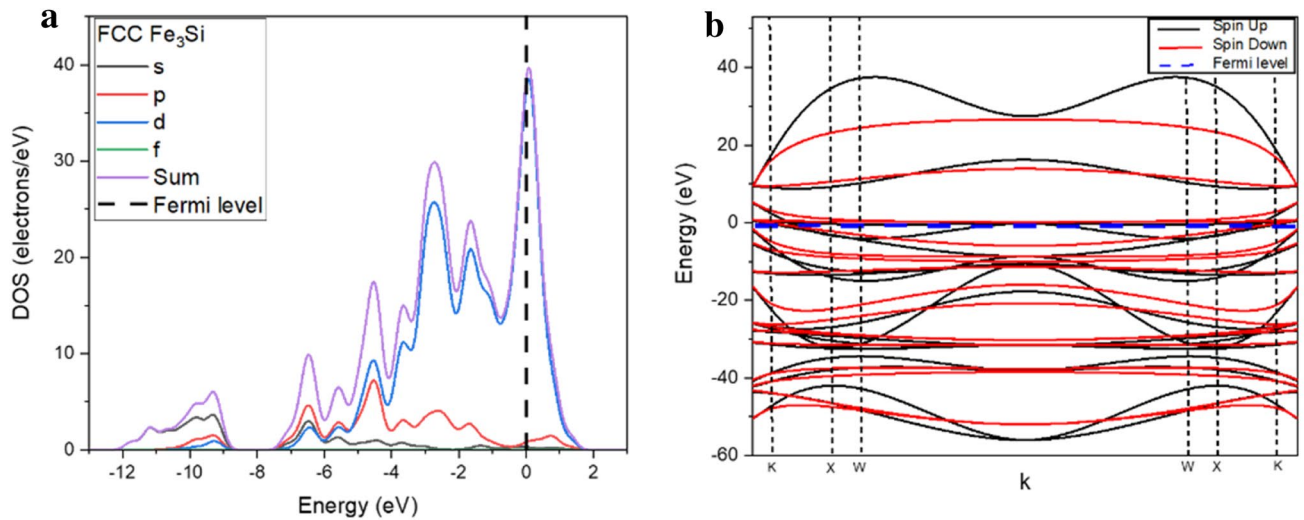


Fig. 9 **a** Total density of states (DOS) and **b** band structure of Fe₃Si (fcc) around the Fermi level (dotted line)

reflects in the spin polarization value which is higher for the fcc phase as shown in Table 1. The bcc phase has a similar behavior than that of the fcc phase; thus, it is possible to conclude from the experimental evidence discussed above that this phase may also be present.

The valence and conduction bands for the sc structure (Fig. 8b) are completely overlapping, which indicates that there is not a separation between different reciprocal lattice points, with a bandgap of 0.392 eV. However, in the band structure (Fig. 9b), the valence and conduction bands are located at different reciprocal lattice points with a bandgap of 0.775 eV. Similar behavior is observed for the bcc phase (Fig. 10b), with overlapping of the band lines that indicates a semiconductor behavior and a pronounced peak in the

vicinity of the characteristic Fermi level of the structures that have magnetization. Thus, it can be concluded that the Fe₃Si phases (fcc and bcc) behave as an indirect bandgap semiconductor, with high stability reflected in its energy gap [31, 32]. In addition, the origin of the magnetization of the fcc and bcc phases of Fe₃Si may be due to the change originating in the spin transfer caused by the electrical change [33].

On the other hand, the FeSi in its primitive phase (sc) would have stable paramagnetic behavior, reflected in its small energy gap. The main peaks centered near the Fermi level are due to the highest occupied states, and the peak just above the Fermi energy is due to the flat band states, and so in this way, the signal of the magnetic transitions

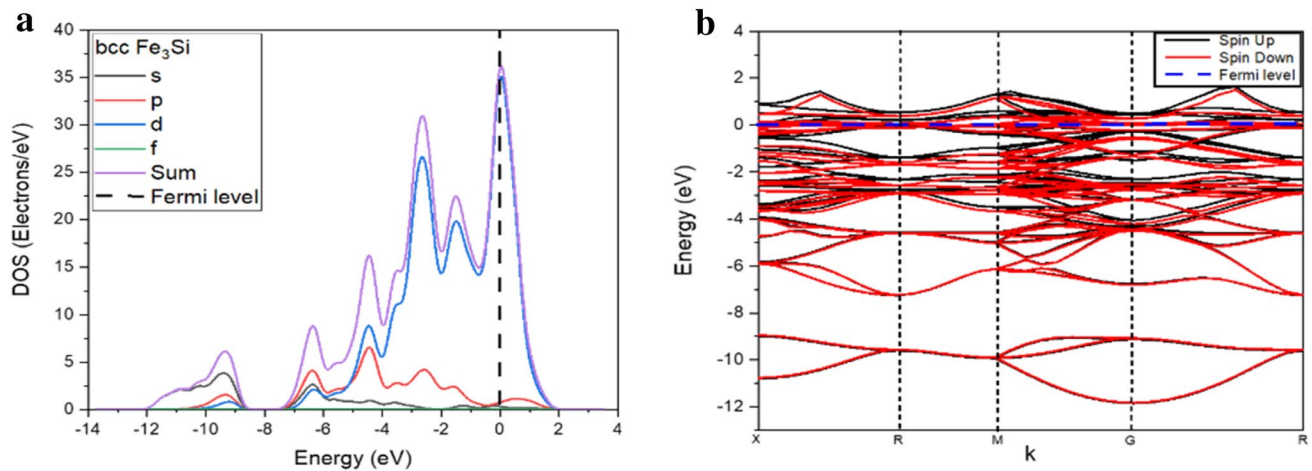


Fig. 10 **a** Total density of states (DOS) and **b** band structure of Fe_3Si (bcc) around the Fermi level (dotted line)

Table 1 Energetic and thermodynamic values for the difference crystallographic phase

	Structure		
	Fe_3Si (fcc)	Fe_3Si (bcc)	FeSi (sc)
Fermi energy (eV)	-8.083	-8.462	-7.272
Gap energy (eV)	0.775	0.778	0.392
Edge of valence band (eV)	-8.471	-8.462	-7.468
Edge of conduction energy (eV)	-7.696	-7.685	-7.075
Spin polarization (eV)	51.659	51.659	20.016
Magnetization (bohr mag/cell)	0.63	2.02	0
Lattice parameter (Å)	5.52	5.52	4.44
Cell volume (Å ³)	167.83	168.164	87.587

in these two phases (fcc and bcc) is presented around the X-point [12].

It can be deduced, from the theoretical results, that the experimental evidence obtained with the Mossbauer spectrometry may be due to the fcc or bcc phase or a combination of both since they have a very pronounced signal near the Fermi level that confirms the magnetization and spin polarization reported in Table 1.

4 Conclusions

The melting and heat treatment process allowed us to consolidate the ordered FeSi (sc) phase, which presents a paramagnetic behavior. The soft magnetic behavior detected by VSM measurement contrasts with the paramagnetic behavior detected by Mossbauer spectrometry. This is explained by the nanostructured character of the sample, in which the atoms of the grain boundaries lost their coherence and can be the formation seed of the Fe_3Si ferromagnetic phase. This was

correlated using theoretical calculations, where it was demonstrated that the presence of Fe_3Si stoichiometry in the fcc and bcc crystalline structures is probable. The magnetic behavior of the detected particles by VSM is confirmed by the Thamm and Hesse plot, which shows that particles present a dipolar magnetic interaction. Electronic properties determination through simulation allowed a deep study of these structures and open different paths to evaluate electric, magnetic, and electrochemical and predict the material behavior in controlled conditions. DFT calculations showed that the highest polarization is presented by the fcc phase, followed by the bcc structure. This is due to their electrons are more localized near the Fermi level, which increases the magnetic moment, as well as a greater number of Fe atoms that contribute to the magnetic moment. The analysis of the band structures revealed that the Fe_3Si (fcc) and bcc crystalline structures have semiconductor behavior and phase stability as compared to the FeSi (sc) phase, which is unstable in its phase.

Acknowledgements The authors would like to thank CENM (Centro de Excelencia en Nuevos Materiales) and Universidad del Valle for their financial support through research project “Study of FeSi (sc) phase and electronic simulation by DFT”. R. Hernández Bravo and J.M González Carmona thanks to Dirección de Cátedras CONACyT for the financial support granted during the elaboration of this manuscript.

Compliance with ethical standards

Conflict of interest The authors declare that they have no conflict of interest.

References

1. A. Reyes, Y. Arredondo, O. Navarro, First principles study of the effects of disorder in the $\text{Sr}_2\text{FeMoO}_6$ perovskite. *Rev. Mex. Física.* **62**(2),160–163 (2016)

2. R. Zeller, Spin-polarized DFT calculations and magnetism. *Comput. Nanosci. do it yourself* **31**, 419 (2006)
3. A. García Escorial et al., Ball milling mechanical alloying in the Fe_{100-x}Si_x system. *Mater. Sci. Eng. A* **134**, 1394–1397 (1991)
4. E. Gaffet, N. Malhouroux, M. Abdellaoui, Far from equilibrium phase transition induced by solid-state reaction in the FeSi system. *J. Alloys Compd.* **194**(2), 339–360 (1993)
5. B. Zuo, T. Sritharan, Ordering and grain growth in nanocrystalline Fe₇₅Si₂₅ alloy. *Acta Mater.* **53**(4), 1233–1239 (2005)
6. J.F. Piamba, R.R. Rodríguez, G.A. Pérez Alcazar, Mössbauer and xrd study of the Fe_{0.5}Si_{0.5} system produced by mechanical alloying and sinterization. *Rev. Mex. Física* **58**(2), 88–92 (2012)
7. W. Moffatt, in *The handbook of binary phase diagrams*, ed. by N.Y. Schenectady. General Electric Co. Corporate Research and Development Technology Marketing Operation (1981)
8. Y. Jing, Y. Xu, J.P. Wang, Fabrication of Heuslar Fe₃Si nanoparticles. *J. Appl. Phys.* **105**(7), 1–4 (2009)
9. M. Shaban, K. Nomoto, S. Izumi, T. Yoshitake, Characterization of near-infrared n-type B-FeSi₂/p-type Si heterojunction photodiodes at room temperature. *Appl. Phys. Lett.* **94**(22), 3–6 (2009)
10. M. Shaban, H. Kondo, K. Nakashima, T. Yoshitake, Electrical and photovoltaic properties of n-type nanocrystalline-FeSi₂/p-type Si heterojunctions prepared by facing-targets direct-current sputtering at room temperature. *Jpn. J. Appl. Phys.* **47**(7 PART 1), 5420–5422 (2008)
11. E.E. Fullerton et al., Magnetic decoupling in sputtered Fe/Si superlattices and multilayers. *J. Appl. Phys.* **73**(10), 6335–6337 (1993)
12. A.I. Al-Sharif, M. Abu-Jafar, A. Qteish, Structural and electronic structure properties of FeSi: the driving force behind the stability of the B20 phase. *J. Phys. Condens. Matter* **13**(12), 2807–2815 (2001)
13. E. Carvajal, R. Oviedo-Roa, M. Cruz-Irisson, O. Navarro, First-principles study of Fe–Mo double perovskites. *Rev. Mex. Fis.* **58**, 171–173 (2012)
14. R. Masrour, A. Jabar, Ground state and magnetic phase transitions of the spin Lieb nanolattice: Monte Carlo simulations. *Phys. A Stat. Mech. Appl.* **491**, 843–851 (2018)
15. Y. Gu, J. He, X. Zhan, Z. Ji, Y. Zhang, C. Zhou, Density functional calculations on electronic and magnetic properties of Fe–Pt systems. *Mater. Sci. Forum* **475–479**(IV), 3103–3106 (2005)
16. V. Cardoso Schwindt, M. Sandoval, J.S. Ardenghi, P. Bechthold, E.A. González, P.V. Jasen, Electronic structure and magnetism on FeSiAl alloy: a DFT study. *J. Magn. Magn. Mater.* **389**, 73–76 (2015)
17. S. Nazir, N. Ikram, S.A. Siddiqi, Y. Saeed, A. Shaukat, A.H. Reshak, First principles density functional calculations of half-metallic ferromagnetism in Zn_{1-x}Cr_xS and Cd_{1-x}Cr_xS. *Curr. Opin. Solid State Mater. Sci.* **14**(1), 1–6 (2010)
18. J. Teillet, F. Varret, Mosfit Program. Unpublished, University of Le Maine
19. A.C. Larson, R.B. Von Dreele, General structure analysis system (GSAS). Los Alamos National Laboratory Report (2004)
20. S.J. Clark et al., First principles methods using CASTEP. *Zeitschrift für Kristallographie* **220**, 567–570 (2005)
21. M.D. Segall et al., First-principles simulation: ideas, illustrations and the CASTEP code. *J. Phys. Condens. Matter* **14**(11), 2717–2744 (2002)
22. A.D. Corso, A.M. Conte, Spin-orbit coupling with ultrasoft pseudopotentials: application to Au and Pt. *Phys. Rev. B* **71**(11), 115106 (2005)
23. N.J. Mosey, E.A. Carter, Ab initio evaluation of Coulomb and exchange parameters for DFT+U calculations. *Phys. Rev. B Condens. Matter Mater. Phys.* **76**(15), 155123 (2007)
24. K. Harun, N.A. Salleh, B. Deghfel, M.K. Yaakob, A.A. Mohamad, DFT + U calculations for electronic, structural, and optical properties of ZnO wurtzite structure: a review. *Results Phys.* **16**, 102829 (2020)
25. J.F. Piamba, G.A. Pérez Alcázar, Effect of disorder on the structural and magnetic properties of the Fe₅₀Si₅₀ nanostructured system. *J. Alloys Compd.* **643**(S1), S297–S301 (2015). <https://doi.org/10.1016/j.jallcom.2014.12.277>
26. W.A. Hines et al., Magnetization studies of binary and ternary alloys based on Fe₃Si. *Phys. Rev. B* **13**(9), 4060–4068 (1976)
27. S. Torkan, A. Ataie, H. Abdizadeh, S. Sheibani, Effect of milling energy on preparation of nano-structured Fe₇₀Si₃₀ alloys. *Powder Technol.* **267**, 145–152 (2014)
28. G.A. Pasquevich, P.M. Zélis, M.B. Van Fernández Raap, F.H. Sánchez, Hyperfine field temperature dependence of Fe₃Si from Mössbauer thermal scans. *Phys. B Condens. Matter* **354**(1), 369–372 (2004)
29. S. Thamm, J. Hesse, A simple plot indicating interactions between single-domain particles. *J. Magn. Magn. Mater.* **154**(2), 254–262 (1996)
30. M.K. Horton, J.H. Montoya, M. Liu, K.A. Persson, High-throughput prediction of the ground-state collinear magnetic order of inorganic materials using density functional theory. *npj Comput. Mater.* (2019). <https://doi.org/10.1038/s41524-019-0199-7>
31. Y. Shin, D. Anh Tuan, Y. Hwang, T. Viet Cuong, S. Cho, Formation and ferromagnetic properties of FeSi thin films. *J. Appl. Phys.* (2013). <https://doi.org/10.1063/1.4800839>
32. K.A. Bush et al., Compositional engineering for efficient wide band gap perovskites with improved stability to photoinduced phase segregation. *ACS Energy Lett.* **3**(2), 428–435 (2018)
33. K.I. Sakai, T. Sonoda, S.I. Hirakawa, K. Takeda, T. Yoshitake, Current-induced magnetization switching in Fe₃Si/FeSi₂ artificial lattices. *Jpn. J. Appl. Phys.* **51**(2 PART 1), 028004 (2012). <https://doi.org/10.1143/JJAP.51.028004>

Publisher's Note Springer Nature remains neutral with regard to jurisdictional claims in published maps and institutional affiliations.